Effect of Fiber Orientation on the Mechanical Performance of Natural Fiber Polymer Composite Bicycle Frame using Finite Element Analysis

Kok Sem Too
Faculty of Engineering, Technology and Built Environment, UCSI University, Kuala Lumpur, 56000, Malaysia

Cik Suhana Hassan
Faculty of Engineering, Technology and Built Environment, UCSI University, Kuala Lumpur, 56000, Malaysia

Nor Fazilah Abdullah
Faculty of Engineering, Technology and Built Environment, UCSI University, Kuala Lumpur, 56000, Malaysia

Ammar Abdulaziz Majeed Al-Talib
Faculty of Engineering, Technology and Built Environment, UCSI University, Kuala Lumpur, 56000, Malaysia

Email: 1001748617@ucsiuniversity.edu.my, suhana@ucsiuniversity.edu.my, norfa@ucsiuniversity.edu.my, ammart@ucsiuniversity.edu.my

Abstract

In this research, the performance of oil palm empty fruit bunch (OPEFB) fiber-reinforced epoxy composite with varying fiber orientation and stacking sequence as the material for mountain bike frame was studied utilizing ANSYS software. The choice of OPEFB fiber was motivated by the fact that the waste by-product of oil palm extraction in Malaysia alone might reach 70-80 million tons per year, with 90% of oil palm biomass lost as waste. The properties of epoxy OPEFB composite in principal 1, 2, and 3 directions were calculated using Whitney and Riley estimates. 10 stacking sequences and five loading conditions were taken. The results show that the fibre orientation of epoxy OPEFB composite on the bicycle frame had little effect on the performance contrary to the number of plies in the laminate or number of laminates which had major effects.

Keywords: Biocomposites, Bicycle frame, Oil palm empty fruit bunch, Polymer composites

1. Introduction

In the 21st century, companies and governments always push towards green technologies, eco-friendly products, and sustainability. In fact, in 2015, Sustainable Development Goals (SDGs) were established by the United Nations (UN) to push for all countries to take part in sustainability for the conservation and preservation of nature and resources for current and future generations [1]. SDGs were fully adopted by the Malaysian government and taught in universities. With this awareness, to reduce the use of resources like fuels and cut carbon emissions, bicycles become the ideal vehicle for short-distance travel.

While it is true that bicycles do not produce emissions, the manufacturing of steel, aluminium, or titanium bicycle frames produces a lot of carbon emissions. With the increasing popularity of bicycles, more bicycles are going to be manufactured and more carbon emissions are going to be produced. In Malaysia, there is also another problem involving the oil palm industry. Oil palm empty fruit bunches (OPEFB) are discarded by the industry as waste in large quantities without utilization [2]. OPEFB fibre has the potential to be used as reinforcing fibre in composite materials. Therefore, utilizing OPEFB fibre in a composite bicycle frame would ease both problems at the same time.

Many researchers have investigated the properties of OPEFB fibre and OPEFB fibre in matrix. Gunawan et al. [3] performed experiment to find out mechanical properties of 40 strands of OPEFB fibre and found that the average Young's modulus is 11.88 GPa and the average tensile strength is 156.3 MPa. Zuhri [4] experimented on just a single strand of OPEFB fibre and found that Young's modulus is 1.7 GPa and tensile strength is 71 MPa. Hassan [5] experimented on

unidirectional OPEFB fibre-reinforced epoxy composite in 0º, 45º, and 90º directions and found that the tensile strengths are 30.5 MPa, 10 MPa, and 9.2 MPa respectively.

Utilizing unidirectional continuous OPEFB fibre in a composite bicycle frame requires the study of the fibre orientation and stacking sequence to produce a bicycle frame that can withstand all loading conditions. As investigated by the researchers, the properties of OPEFB fibre are adequate for the development of composite bicycle frames.

2. Methodology

2.1. *Mountain bicycle frame*

The dimensions and geometry of the mountain bicycle frame was adopted from a journal by Sajimsha B et al. [6]. The modelling of the frame was completed on SOLIDWORKS. Table 1 shows the parameters of dimensions and geometry of the bicycle frame.

Table 1. Parameters of dimensions and geometry of the mountain bicycle frame

Parameter	Value
Head tube angle	73.5º
Seat tube angle	73.5º
Top tube length	580 mm
Seat tube length	570 mm
Chain stay length	360 mm
Head tube length	120 mm

For composite material simulation, the shell model of the bicycle frame was exported to ANSYS. The meshing was done on ANSYS Mechanical and the completed meshed model has 12830 nodes and 12306 elements. Fig. 1 shows the completed meshed model of the bicycle frame.

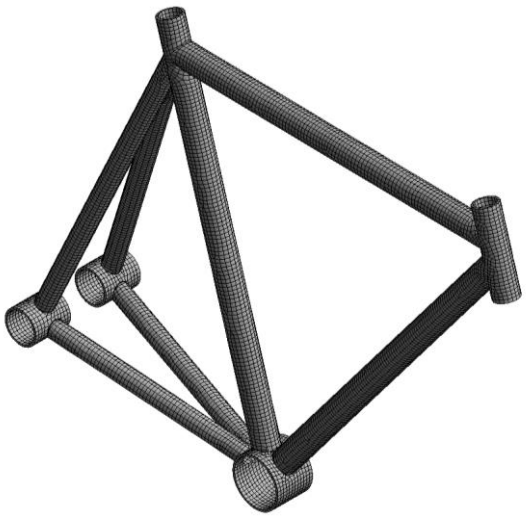

Fig.1 Shell model of mountain bicycle frame

2.2. *OPEFB fiber reinforced epoxy composite properties*

Although many researchers have conducted experiments on the properties of OPEFB fibre reinforced epoxy composite, only the properties of Young's modulus, tensile strength, and flexural strength were found. Properties such as shear modulus and Poisson's ratio in principal 1-2, 2-3, and 1-3 directions and compressive strength and shear strength in principal 1, 2, and 3 directions were not found. To find the moduli and Poisson's ratios in all three directions of composite, many theoretical estimates were developed. One such theoretical estimates is Whitney and Riley estimates developed by Air Force Materials Laboratory [7-8]. The calculations of the moduli and Poisson's ratios using Whitney and Riley theory are less rigorous than other theoretical estimates and only require Young's modulus, shear moduli, bulk moduli and Poisson's ratios of the fibre and matrix. The theory also regards that the fibre and matrix are isotropic. The compressive strength and shear strength of the composite were calculated using the equations in Chapter 5 of the book of Engineering Mechanics of Composite Materials by Daniel and Ishai [9]. The properties of OPEFB fibre were obtained from an experiment done by Gunawan et al. [3] and the properties of epoxy were obtained from Appendix A in the book [9]. Table 2 shows the calculated properties of the epoxy OPEFB composite. Note that the fibre-to-matrix volume ratio is 60:40.

Table 2. OPEFB fibre properties

Young's modulus 1 (GPa)	8.848
Young's modulus 2 (GPa)	6.347
Young's modulus 3 (GPa)	6.347
Poisson's ratio 1-2	0.3184
Poisson's ratio 2-3	0.32
Poisson's ratio 1-3	0.3184
Shear modulus 1-2 (GPa)	2.899
Shear modulus 2-3 (GPa)	2.404
Shear modulus 1-3 (GPa)	2.899
Bulk Modulus (GPa)	5.937
Tensile strength 1 (MPa)	142 MPa
Tensile strength 2 (MPa)	49.46 MPa
Tensile strength 3 (MPa)	49.46 MPa
Compressive Strength 1 (MPa)	400 MPa
Compressive Strength 2 (MPa)	143.4
Compressive Strength 3 (MPa)	143.4
Shear Strength 1-2 (MPa)	70.82
Shear Strength 2-3 (MPa)	48
Shear Strength 1-3 (MPa)	70.82

2.3. *Stacking sequence*

The stacking sequences of the plies were determined from the journal of Thomas Jin-Chee LIU et al. [10] who found 10 stacking sequences of 8-ply laminate that

produced better designs for composite bicycle frames. The 10 stacking sequences are shown in Table 3. Each stacking sequence is designated with a letter with 0, 45 and 90 indicating the fibre orientation angle in the composite. Fig. 2 shows examples of 0º fibre orientation and 90º fibre orientation on the bottom bracket.

Table 3. Composite stacking sequence

Designation	Stacking Sequence
A	$[0/90/45/-45]_s$
B	$[0/90/-45/45]_s$
C	$[90/0/45/-45]_s$
D	$[90/0/-45/45]_s$
E	$[-45/45/0/90]_s$
F	$[-45/45/90/0]_s$
G	$[45/-45/0/90]_s$
H	$[45/-45/90/0]_s$
I	$[0/90/90/0]_s$
J	$[90/0/0/90]_s$

Thomas Jin-Chee LIU [10] used the same stacking sequence of 8-ply laminate for the entire bicycle frame. Other studies are more dynamic with having different stacking sequence and number of plies for each section of the bicycle frame. For instance, Hu et al. [11] separated the bicycle frame into two sections: section A with 8-ply laminate consisting of head tube, top tube, seat tube, and bottom bracket and section B with 5-ply laminate consisting of seat stays and chain stays. Jung et al. [12] initially used the same stacking sequence of 8-ply laminate for the entire bicycle frame then separated the bicycle frame based on the weak regions and failure indexes into three sections with different stacking sequences and 16-ply laminate only for section 3. Jung et al. [12] grouped the head tube into Group 1, top tube, seat stays, and chain stays into Group 2, and seat tube, top tube, and bottom bracket into Group 3. Similarly, Chun et al. [13] initially employed the same stacking sequence of 20-ply laminate throughout the bicycle frame and then optimised different stacking sequences for each member of the frame based on the initial results.

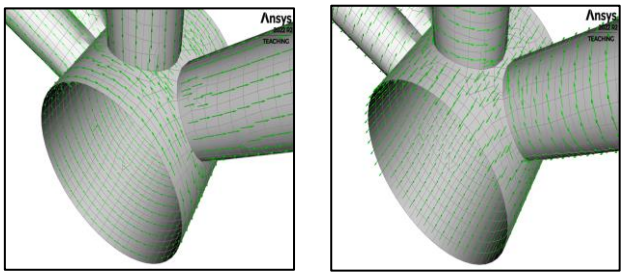

a. 0° b. 90°

Fig. 2. Fibre orientation angle

2.4. *Loading conditions*

The bicycle frame design and loading conditions applied were based on Sajimsha B et al. [7] work. There were five loading conditions simulated and analysed. All the loading conditions are shown in Fig. 3. The first loading condition is static start-up. It simulates the bicycle in a resting state with a rider sitting on the saddle and the rider is about to start pedalling. A force of 700 N is applied to the top of the seat tube implying the weight of the rider and a force of 200 N is applied to the bottom bracket implying pedalling force. The head tube and rear brackets are fixed supported. The second loading condition is steady state pedalling. It simulates the bicycle is being pedalled out of saddle, meaning that the rider is not sitting on the saddle instead standing up while pedalling. Force of 1000 N is applied to the top of the head tube implying the force of the rider's hands pushing down on the steering and force of 200 N is applied to the bottom bracket implying the pedalling force. The head tube and rear brackets are fixed supported. The third loading condition is vertical impact. It is to simulate an event of impact to the top of the seat tube. Downward force of 2250 N is applied to the top of the seat tube. The head tube and rear brackets are fixed supported. The fourth loading condition is horizontal impact. Similarly to third loading condition, it simulates an event of impact to the top tube. Horizontal force of 2250 N is applied along the top tube. The head tube and rear brackets are fixed supported. The fifth loading condition is rear wheel braking. It simulates the rider is applying brake to the rear wheel when coming to a stop. Horizontal force of 750 N is applied to each of the rear bracket. The bottom bracket is fixed supported.

To analyse whether the bicycle frame fails or not in a loading condition, multiple composite failure theories were selected in composite failure tool on ANSYS. ANSYS calculates the failure theories based on inverse reserve factor (IRF) which tells a number that indicates failure. IRF between 0 and 0.99 indicates that the bicycle frame is still intact while IRF that exceeds 1 indicates the bicycle frame already fails. Composite failure theories can be divided into three groups. Limit or noninteractive theories like maximum stress and maximum strain theories disregard interaction among different stress components and only compare individual ply stresses or strain with the corresponding ultimate strengths or strains [9]. Interactive theories like Tsai-Hill and Tsai-Wu theories include all stress component in one expression without reference to particular failure modes 9. Partially interactive or failure-mode-based theories like Hashin and Puck theories give separate criteria for fibre and interfibre failures [9]. Five failure theories are chosen in the composite failure tool: Maximum stress theory, Tsai-Wu theory, Tsai-Hill theory, Hashin theory, and Puck theory.

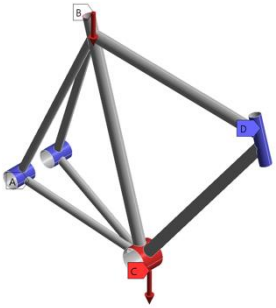

(a) Static start-up

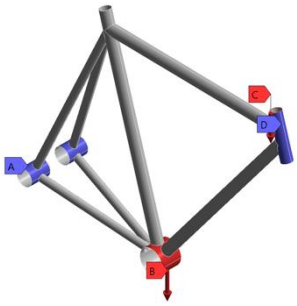

(b) Steady-state pedalling

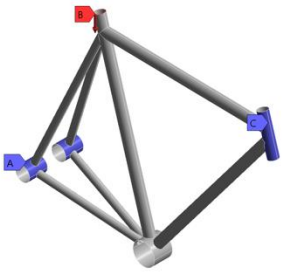

(c) Vertical impact

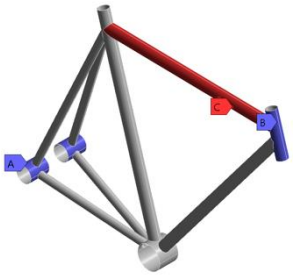

(d) Horizontal impact

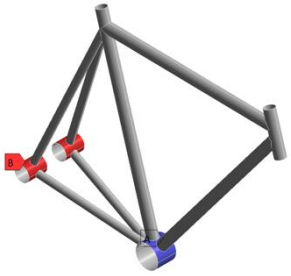

(e) Rear-wheel braking

Fig. 3. Loading conditions applied

3. Results and Discussion

3.1. *Initial analysis*

The initial equivalent (von-mises) stress results show good or even better performances than those of the conventional materials for some stacking sequences and loading conditions. All the stress values for corresponding stacking sequences and loading conditions are shown in Table 4. For comparison, the equivalent (von-mises) stress results produced by Deepak [14] were listed in Table 5.

Table 4. Initial equivalent (von-Mises) stress

	Static Start-up	**Steady State Pedalling**	**Vertical Impact**	**Horizon-tal Impact**	**Rear Wheel Braking**
A	11.242	4.5884	35.034	11.127	40.049
B	11.245	4.5864	35.051	11.128	40.148
C	9.7708	3.7435	30.249	8.0981	**32.523**
D	**9.7704**	3.7417	**30.248**	8.0976	33.298
E	10.248	4.149	31.733	9.3719	34.823
F	10.259	4.2497	31.768	9.3758	35.377
G	10.235	4.1446	31.695	9.4727	38.412
H	10.245	4.2379	31.728	9.4773	38.717
I	11.196	4.6299	34.896	10.994	40.239
J	9.7798	**3.6939**	30.279	**7.9794**	32.685

Table 5. Equivalent (von-Mises) stress of conventional materials

	Static Start-up	**Steady State Pedalli-ng**	**Vertic al Impac t**	**Horizo ntal Impac t**	**Rear Wheel Brakin-g**
Steel	9.8212	6.3773	31.216	28.069	17.746
Aluminium	10.915	7.4270	33.722	30.364	17.780
Titanium	10.896	7.3168	34.607	31.071	18.022
Carbon Fibre	10.940	10.940	34.839	33.941	19.498

In static start-up, stacking sequence C, D, and J have lower stresses than all the conventional materials. Stacking sequence E, F, G, and H have lower stresses than aluminium 6061 T6, titanium grade 9 and carbon fibre while stacking A, B, and I have higher stresses than all the conventional materials. In steady state pedalling, all the stacking sequences show lower stresses than all the conventional materials. In vertical impact, stacking sequence C, D, and J have lower stresses than steel while stacking sequence E, F, G, and H have lower stresses than aluminium 6061 T6, titanium grade 9 and carbon fibre. Stacking sequence A, B, and H have higher stresses than all the conventional materials. In Horizontal impact, all the stacking sequences have lower stresses than all the conventional materials contrary to rear wheel braking

condition which displays that all the stacking sequences have higher stresses than all the conventional materials.

In each of the loading condition, the maximum stress is always concentrated at the same region despite the different stacking sequences. As can be seen in Fig. 4, the stress concentration is at the connection between seat tube and seat stays in static start-up; connection between down tube and bottom bracket in steady state pedalling; connection between seat tube and seat stays in vertical impact; connection between heat tube and top tube in horizontal impact; intersection between chain stays in rear wheel braking.

The bicycle frame will not necessarily fail at the stress concentration region. The region may be able to hold the maximum stress while other regions may not be able to hold their lower stresses. This is further seen with the location of maximum inverse reserve factor.

The initial total deformation results in Table 6 are not comparable to the results of the conventional materials in Table 7. As expected, the deformation in each loading condition and stacking sequence is way higher than the deformations for all the conventional materials. This is due to the epoxy OPEFB composite having way lower tensile and compressive moduli than all the conventional materials. Thus, producing way higher deformations. The deformations in rear wheel braking condition are unacceptable as 6 mm deformation is too high and will possibly affect riding performance and stability. As observed as well the different in deformations between the stacking sequences in each loading condition is insignificant.

Table 6. Initial total deformation induced.

	Static Start-up	Steady State Pedalling	Vertical Impact	Horizon-tal Impact	Rear Wheel Braking
A	0.29322	**0.13132**	0.8982	0.25591	6.8875
B	0.29323	0.1314	0.89823	0.25591	6.8863
C	0.29325	0.13792	0.89828	0.25626	6.8907
D	0.29325	0.13801	0.89829	0.25626	6.8895
E	0.29334	0.13446	0.89861	0.25608	6.8894
F	0.2932	0.13663	0.89812	0.25618	6.8824
G	0.29333	0.1342	0.89859	0.25608	6.8927
H	0.29318	0.13636	0.89808	0.25617	6.886
I	**0.29066**	0.13167	**0.89057**	**0.25316**	**6.8304**
J	0.29083	0.13614	0.89113	0.25341	6.8401

Table 7. Total deformation of conventional materials

	Static Start-up	Steady State Pedalling	Vertical Impact	Horizontal Impact	Rear Wheel Braking
Steel	0.0081404	0.0084963	0.024997	0.030902	0.18428
Aluminium 6061 6T	0.023512	0.024481	0.072276	0.090021	0.52604
Titanium Grade 9	0.017838	0.018578	0.054793	0.068393	0.39739
Carbon Fibre	0.0040985	0.0042668	0.012585	0.015749	0.089395

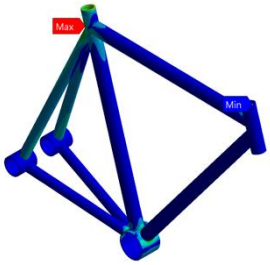

(a) Static start-up

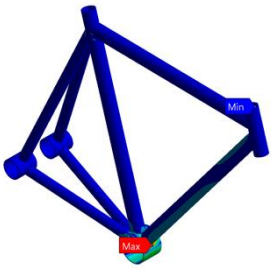

(b) Steady-state pedalling

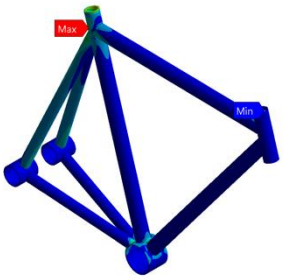

(c) Vertical impact

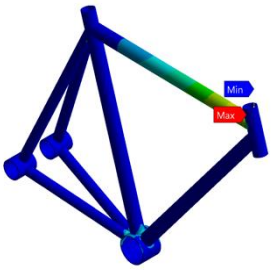

(d) Horizontal impact

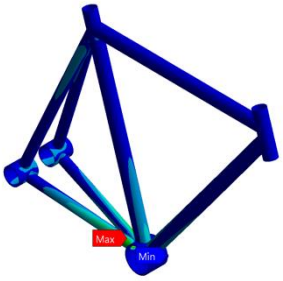

(e) Rear-wheel braking

Fig. 4. Stress concentration of each loading condition

Similarly to stress concentration, the bicycle frame deforms at the same location in each loading condition regardless of the stacking sequences. The bicycle frame always deforms the most at the highest load location if there is no fixed support at the location. The bicycle frame deforms at the tip of the seat tube where force of 700 N is applied in static start-up; bottom bracket where force of 200 N is applied in steady state pedalling; tip of the seat tube where force of 2250 N is applied in vertical impact, connection between top tube and seat tube where force of 2250 N is applied to the top tube in horizontal impact; both rear brackets where force of 750 N is applied to each in rear wheel braking.

Inverse reserve factor (IRF) is an indication if the bicycle frame will fail under the loading conditions. If the inverse reserve factor exceeds 1, the bicycle frame will fail. As can be observed in Table 8, the bicycle frame has relatively low IRF in static start-up and steady state pedalling but high IRF in vertical impact, horizontal impact, and rear wheel braking, indicating that the frame will most likely fail under these loading conditions.

Table 8. Initial inverse reserve factor

	Static Start-up	Steady State Pedalling	Vertical Impact	Horizon-tal Impact	Rear Wheel Braking
A	0.15252	0.09564	0.52981	0.2719	0.6079
B	0.15182	0.095529	0.54129	0.27586	0.61455
C	0.20657	0.13149	0.80163	0.34544	0.84844
D	0.20922	0.13133	0.81165	0.34912	0.85809
E	0.20234	0.11412	0.80113	0.35434	0.80075
F	0.20584	0.11701	0.81488	0.35861	0.81305
G	0.15299	0.11521	0.5253	0.27102	0.71251
H	0.1565	0.11821	0.53666	0.27416	0.72179
I	0.15032	0.096605	0.53767	0.27396	0.61409
J	0.20484	0.12935	0.7955	0.34325	0.84165

The stacking sequence A, B, G, H, and I have slightly higher IRF than 0.15 compared to stacking sequence C, D, E, F, and J that have IRF higher than 0.2 in static start-up. Stacking sequence A, B and I have IRF lower than 0.1, stacking sequence E, F, G, H have IRF slight higher than 0.11, and stacking sequence C, D, and J have IRF higher than 0.12 in steady state pedalling.

Stacking sequence A, B, G, H, I have slightly higher IRF than 0.5 while stacking sequence C, D, E, F, and J have IRF around 0.8 in vertical impact. Stacking sequence A, B, G, H, and I have IRF slightly higher than 0.27 while Stacking sequence C, D, E, F, and J have IRF higher than 0.34. Lastly, Stacking sequence A, B, and I have slightly higher IRF than 0.6, stacking sequence G and H have IRF slight higher than 0.7, and stacking sequence C, D, E, F, and J have slight higher IRF than 0.8. General trend can be seen here is that stacking sequence A, B, G, H, and I produce lower IRF than all the other stacking sequences in all loading conditions. For initial results, stacking sequence A, B, G, H, and I are chosen to be general good stacking sequences. Table 9 shows the top five stacking sequences in each loading condition and they are composed of stacking sequences A, B, G, H and I except for steady state pedalling that swaps stacking sequence H for E. The (a), (b), (c) and (d) are indicators for the location of the maximum IRF which occurs at only four locations; as shown in Fig. 5. Location a is the connection between seat tube and chain stays; location b is the connection between bottom bracket and seat tube; location c is the connection between bottom bracket and down tube; location d is the chain stays intersection. These locations are also the weak regions of the bicycle frame. The designation inside the bracket beside the IRF value is the location of the IRF. The maximum IRF is greatly influenced by loading conditions but not the stacking sequences except for static start-up which shows variation in the maximum IRF locations based on the stacking sequences.

Table 9. Top five stacking sequences of each loading condition for IRF

Static Start-up	
$[0/90/90/0]_s$	0.15032 (a)
$[0/90/-45/45]_s$	0.15182 (a)
$[0/90/45/-45]_s$	0.15252 (a)
$[45/-45/0/90]_s$	0.15299 (c)
$[45/-45/90/0]_s$	0.1565 (c)
Steady State Pedalling	
$[0/90/-45/45]_s$	0.09552 (c)
$[0/90/45/-45]_s$	0.09564 (c)
$[0/90/90/0]_s$	0.09660 (c)
$[-45/45/0/90]_s$	0.11412 (c)
$[45/-45/0/90]_s$	0.11521 (c)
Vertical Impact	
$[45/-45/0/90]_s$	0.5253 (b)
$[0/90/45/-45]_s$	0.52981 (b)
$[45/-45/90/0]_s$	0.53666 (b)
$[0/90/90/0]_s$	0.53767 (b)
$[0/90/-45/45]_s$	0.54129 (b)
Horizontal Impact	
$[45/-45/0/90]_s$	0.27102 (b)
$[0/90/45/-45]_s$	0.2719 (b)
$[0/90/90/0]_s$	0.27396 (b)
$[45/-45/90/0]_s$	0.27416 (b)
$[0/90/-45/45]_s$	0.27586 (b)
Rear Wheel Braking	
$[0/90/45/-45]_s$	0.6079 (d)
$[0/90/90/0]_s$	0.61409 (d)
$[0/90/-45/45]_s$	0.61455 (d)
$[45/-45/0/90]_s$	0.71251 (d)
$[45/-45/90/0]_s$	0.72179 (d)

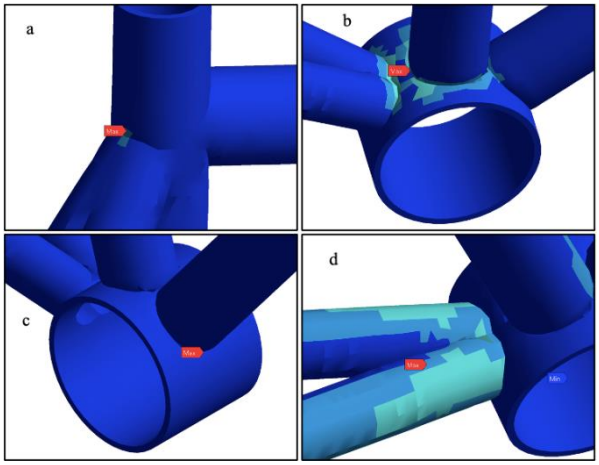

Fig. 5. Locations of maximum inverse reserve factor

3.2. *Optimization*

It was obvious that only one laminate of epoxy OPEFB composite cannot be feasible for a good performance bicycle frame. The deformation was too high compared to those of conventional materials and especially in rear wheel braking with one laminate. The IRFs in vertical impact, horizontal impact, and rear wheel braking were also high with one laminate. To reduce the deformation and the IRF, another laminate of 8-ply was introduced, creating two 8-ply laminates or 16 plies all together for every member of the bicycle frame.

The results, as shown in Table 10, 11 and 12, show reduction in half for all the stresses, deformations, and IRFs in all the loading conditions. The equivalent (von-Mises) stress was averagely reduced by 50.63% in static start-up; 65.39% in steady state pedalling; 49.95% in vertical impact; 41.55% in horizontal impact; 47.44% in rear wheel braking. The deformation was averagely reduced by 57.13% in static start-up; 71.56% in steady state pedalling; 57.68% in vertical impact; 51.79% in horizontal impact; 60.56% in rear wheel braking. The IRF was averagely reduced by 61% in static start-up; 70.98% in steady state pedalling; 59% in vertical impact; 63.69% in horizontal impact; 53.79% in rear wheel braking.

Table 10. Equivalent (von-Mises) stress results for double-laminate bicycle frame

Designation	Stacking Sequence	Equivalent (von-Mises) Stress (MPa)				
		Static Start-up	Steady State Pedalling	Vertical Impact	Horizontal Impact	Rear Wheel Braking
A_2	$[(0/90/45/-45)_2]_s$	5.1762	1.4255	16.136	5.3502	18.09
B_2	$[(0/90/-45/45)_2]_s$	5.1765	1.4256	16.138	5.3502	18.101
G_2	$[(45/-45/0/90)_2]_s$	4.5443	1.2326	14.397	4.5508	17.234
H_2	$[(45/-45/90/0)_2]_s$	4.5447	1.2382	14.458	4.5512	17.242
I_2	$[(0/90/90/0)_2]_s$	5.1473	1.4184	16.047	5.2871	18.002

Table 11. Total deformation results for double-laminate bicycle frame

Designation	Stacking Sequence	Total Deformation (mm)				
		Static Start-up	Steady State Pedalling	Vertical Impact	Horizontal Impact	Rear Wheel Braking
A_2	$[(0/90/45/-45)_2]_s$	0.12546	0.037708	0.37937	0.12315	2.7109
B_2	$[(0/90/-45/45)_2]_s$	0.12546	0.037705	0.37937	0.12315	2.7109
G_2	$[(45/-45/0/90)_2]_s$	0.12554	0.037838	0.37961	0.12317	2.7131
H_2	$[(45/-45/90/0)_2]_s$	0.12557	0.037923	0.37972	0.12319	2.7139
I_2	$[(0/90/90/0)_2]_s$	0.12437	0.037415	0.37618	0.1218	2.6907

Table 12. Inverse reference factor for double-laminate bicycle frame

Designation	Stacking Sequence	Inverse Reference factor				
		Static Start-up	Steady State Pedalling	Vertical Impact	Horizontal Impact`	Rear Wheel Braking
A_2	$[(0/90/45/-45)_2]_s$	0.060172 (b)	0.029942 (c)	0.2185 (b)	0.097273 (b)	0.30854 (d)
B_2	$[(0/90/-45/45)_2]_s$	0.060416 (b)	0.029935 (c)	0.21947 (b)	0.097597 (b)	0.30946 (d)
G_2	$[(45/-45/0/90)_2]_s$	0.0583 (b)	0.030153 (c)	0.21787 (b)	0.10033 (b)	0.29258 (d)
H_2	$[(45/-45/90/0)_2]_s$	0.058772 (b)	0.030249 (c)	0.21958 (b)	0.10081 (b)	0.29281 (d)
I_2	$[(0/90/90/0)_2]_s$	0.060352 (b)	0.029821 (c)	0.21942 (c)	0.097409 (c)	0.30814 (d)

While all the stresses, deformations, and IRFs were reduced half by just adding an additional laminate, the bicycle frame still had the same stacking sequence throughout. Different stacking sequences for different members of the bicycle frame is proven to be beneficial for sustaining different loading conditions. Therefore, based on the weak regions, the bicycle frame was sectioned into three sections: section 1 consists of top tube, head tube, and down tube; section 2 consists of seat tube alone; section 3 consists of seat stays, chain stays, bottom bracket, and rear brackets. Section 1 would employ stacking sequence B_2 and I_2, section 2 would employ stacking sequence A_2, B_2, G_2, and I_2, and section 3 would employ stacking sequence A_2, and H_2. The combinations of all the stacking sequences of each section are clearly listed in Table 13.

Table 13. Stacking sequences for section 1, 2, and 3

Stacking	Section 1	Section 2	Section 3
K	$[(0/90/90/0)_2]_s$	$[(0/90/90/0)_2]_s$	$[(45/-45/90/0)_2]_s$
L	$[(0/90/90/0)_2]_s$	$[(0/90/90/0)_2]_s$	$[(0/90/45/-45)_2]_s$
M	$[(0/90/90/0)_2]_s$	$[(0/90/-45/45)_2]_s$	$[(45/-45/90/0)_2]_s$
N	$[(0/90/90/0)_2]_s$	$[(0/90/-45/45)_2]_s$	$[(0/90/45/-45)_2]_s$
O	$[(0/90/90/0)_2]_s$	$[(0/90/45/-45)_2]_s$	$[(45/-45/90/0)_2]_s$
P	$[(0/90/90/0)_2]_s$	$[(0/90/45/-45)_2]_s$	$[(0/90/45/-45)_2]_s$
Q	$[(0/90/90/0)_2]_s$	$[(45/-45/0/90)_2]_s$	$[(45/-45/90/0)_2]_s$
R	$[(0/90/90/0)_2]_s$	$[(45/-45/0/90)_2]_s$	$[(0/90/45/-45)_2]_s$
S	$[(0/90/-45/45)_2]_s$	$[(0/90/90/0)_2]_s$	$[(45/-45/90/0)_2]_s$
T	$[(0/90/-45/45)_2]_s$	$[(0/90/90/0)_2]_s$	$[(0/90/45/-45)_2]_s$
U	$[(0/90/-45/45)_2]_s$	$[(0/90/-45/45)_2]_s$	$[(45/-45/90/0)_2]_s$
V	$[(0/90/-45/45)_2]_s$	$[(0/90/-45/45)_2]_s$	$[(0/90/45/-45)_2]_s$
W	$[(0/90/-45/45)_2]_s$	$[(0/90/45/-45)_2]_s$	$[(45/-45/90/0)_2]_s$
X	$[(0/90/-45/45)_2]_s$	$[(0/90/45/-45)_2]_s$	$[(0/90/45/-45)_2]_s$
Y	$[(0/90/-45/45)_2]_s$	$[(45/-45/0/90)_2]_s$	$[(45/-45/90/0)_2]_s$
Z	$[(0/90/-45/45)_2]_s$	$[(45/-45/0/90)_2]_s$	$[(0/90/45/-45)_2]_s$

Equivalent (von-Mises) stress results, as shown in Table 14, show insignificant difference between the stacking sequences except for a few stacking sequences in some loading condition. Stacking sequence Q and Y have lower stresses slightly above 4.5 MPa compared to the rest of the stacking sequences that have stresses slightly above 5 MPa in static start-up. All the stacking sequences in steady state pedalling have stresses slightly above 1.4 MPa and the difference between each other is insignificant. Stacking sequence Q and Y have stresses slightly above 14.3 MPa, stacking sequence R and Z have stresses slightly above 15.5 MPa, and all other stacking sequences have stresses slightly above 16 MPa in vertical impact. In horizontal impact, stacking sequence L, K, N,

P, R, M, O, and Q have stresses slight above 5.28 MPa and stacking sequence T, S, V, X, Z, and U have stresses slightly above 5.35. In rear wheel braking, stacking sequence K, S, M, O, Q, U, W, and Y have stresses slightly above 17.24 MPa and stacking sequence V, X, Z, N, P, R, T, and L have stresses slightly above 18.09 MPa. The stresses are not improved over the stresses of the same case of double-laminate bicycle frame.

Table 14. Equivalent (von-Mises) stress results for double-laminate sectioned bicycle frame

	Static Start-up	Steady State Pedalling	Vertical Impact	Horizon-tal Impact	Rear Wheel Braking
K	5.1354	1.4279	16.009	5.2887	17.241
L	5.1469	1.4218	16.044	5.2881	18.093
M	5.1607	1.429	16.091	5.2892	17.242
N	5.1722	1.4229	16.126	5.2887	18.091
O	5.159	1.429	16.085	5.2892	17.242
P	5.1709	1.4229	16.121	5.2887	18.091
Q	4.5435	1.429	14.397	5.2893	17.242
R	5.0339	1.4229	15.543	5.2887	18.091
S	5.1407	1.4306	16.023	5.3502	17.241
T	5.1521	1.4245	16.059	5.3497	18.091
U	5.166	1.4316	16.105	5.3508	17.242
V	5.1775	1.4255	16.141	5.3502	18.09
W	5.1643	1.4316	16.1	5.3508	17.242
X	5.1762	1.4255	16.136	5.3502	18.09
Y	5.1354	1.4279	16.009	5.2887	17.241
Z	5.1469	1.4218	16.044	5.2881	18.093

Similar trend is observed for the total deformation for double-laminate sectioned bicycle frame, as shown in Table 15. The deformation difference between the stacking sequences in each loading condition is very insignificant. The deformations do not see any improvement over the deformations of the same case of double-laminate bicycle frame. IRFs also do not see any improvement over the IRFs of the same case of double-laminate bicycle frame. The IRF difference between stacking sequences in each loading condition is very insignificant, as shown in Table 16.

Table 15. Total deformation results for double-laminate sectioned bicycle frame

	Static Start-up	Steady State Pedalling	Vertical Impact	Horizon-tal Impact	Rear Wheel Braking
K	0.12515	0.037681	0.37848	0.12185	2.7085
L	0.1251	0.037485	0.3783	0.12181	2.7057
M	0.12536	0.037711	0.37918	0.12188	2.7113
N	0.12531	0.037515	0.379	0.12184	2.7085
O	0.12536	0.037709	0.37918	0.12188	2.7113
P	0.12531	0.037514	0.379	0.12184	2.7085
Q	0.1254	0.037709	0.37929	0.12188	2.7114
R	0.12534	0.037514	0.37911	0.12184	2.7086
S	0.1253	0.037874	0.37884	0.12315	2.7108
T	0.12525	0.037678	0.37867	0.12311	2.708
U	0.12552	0.037904	0.37955	0.12318	2.7137
V	0.12546	0.037708	0.37937	0.12315	2.7109
W	0.12552	0.037903	0.37954	0.12319	2.7137
X	0.12546	0.037707	0.37937	0.12315	2.7109
Y	0.12555	0.037902	0.37965	0.12319	2.7138
Z	0.1255	0.037707	0.37948	0.12315	2.711

Table 16. Inverse reserve factor for double-laminate sectioned bicycle frame

	Static Start-up	Steady State Pedalling	Vertical Impact	Horizon-tal Impact	Rear Wheel Braking
K	0.05958 (b)	0.029985 (c)	0.22218 (b)	0.10058 (b)	0.29283 (d)
L	0.06072 (b)	0.029894 (c)	0.22028 (b)	0.09677 (b)	0.3086 (d)
M	0.05919 (b)	0.03 (c)	0.22057 (b)	0.10025 (b)	0.29282 (d)
N	0.06034 (b)	0.02991 (c)	0.21869 (b)	0.09647 (b)	0.30858 (d)
O	0.05918 (b)	0.03 (c)	0.22061 (b)	0.10024 (b)	0.29282 (d)
P	0.06034 (b)	0.029909 (c)	0.21873 (b)	0.09645 (b)	0.30857 (d)
Q	0.05900 (b)	0.03 (c)	0.22007 (b)	0.10006 (b)	0.29282 (d)
R	0.06016 (b)	0.029909 (c)	0.21818 (b)	0.09626 (b)	0.30857 (d)
S	0.05942 (b)	0.030027 (c)	0.22194 (b)	0.10144 (b)	0.29282 (d)
T	0.06056 (b)	0.029935 (c)	0.22004 (b)	0.09759 (b)	0.30857 (d)
U	0.05902 (b)	0.030042 (c)	0.22033 (b)	0.1011 (b)	0.29281 (d)
V	0.06017 (b)	0.029951 (c)	0.21845 (b)	0.09729 (b)	0.30855 (d)
W	0.05902 (b)	0.030042 (c)	0.22037 (b)	0.10109 (b)	0.29281 (d)
X	0.0601 (b)	0.02995 (c)	0.21849 (b)	0.09727 (b)	0.30854 (d)
Y	0.0595 (b)	0.029985 (c)	0.22218 (b)	0.10058 (b)	0.29283 (d)
Z	0.0607 (b)	0.029894 (c)	0.22028 (b)	0.09677 (b)	0.3086 (d)

Overall, different stacking sequence for each section of the bicycle frame does not produce any improvement at all for epoxy OPEFB composite mountain bicycle frame in this study. Major improvement of equivalent (von-Mises) stresses, total deformations, and inverse reserve factor are seen with addition of laminate or ply. Unlike other studies which found that major improvement of performance by applying different stacking sequence to different member of the bicycle frame, all the other studies used synthetic fibre such as carbon fibre and glass fibre which, in a composite, possess big difference between the Young's modulus 1 and 2, and tensile strength 1 and 2. As calculated by using Whitney and Riley theory, epoxy OPEFB composite does not have very big difference between the properties in principal 1 and 2 direction. Therefore, the fibre orientation of epoxy OPEFB composite in each section of the bicycle frame does not contribute much to the performance compared to the fibre orientation of the entire bicycle frame which saw some improvement in the initial results.

4. Conclusion

The fibre orientation and stacking sequences of epoxy OPEFB composite on mountain bicycle frame have been studied thoroughly. A total of 10 stacking sequences were adopted from previous research. It was found that of the

10 stacking sequences, five stacking sequences, $[0/90/45/-45]_s$, $[0/90/-45/45]_s$, $[45/-45/0/90]_s$, $[45/-45/90/0]_s$, and $[0/90/90/0]_s$, were found to be general good stacking sequences. But the deformations and IRFs of the five stacking sequences in some loading conditions were still high. Therefore, the additional laminate was introduced and the results showed significant reduction by half in stresses, deformations, and IRF. The bicycle frame was also sectioned for employment of different stacking sequence in each section but the results showed no improvement. Hence, for epoxy OPEFB composite bicycle frame, additional laminate or ply will improve the performance significantly but not employment of different stacking sequence in each member of the frame.

Acknowledgements

The authors would like to express their gratitude towards the engineering faculty of UCSI University.

References

1. P. Pradhan, L. Costa, D. Rybski, W. Lucht, and J.P. Kropp, A Systematic Study of Sustainable Development Goal (SDG) Interactions, Earth's Future, 5, 2017, pp. 1169-1179.
2. M.K. Faizi, A.B. Shahriman, M.S. Abdul Majid, B.M.T. Shamsul, Y.G. Ng, S.N. Basah, E.M. Cheng, M. Afendi, M.R. Zuradzman, Khairunizam Wan and D. Hazry, An Overview of the Oil Palm Empty Fruit Bunch (OPEFB) Potential as Reinforcing Fibre in Polymer Composite for Energy Absorption Applications, MATEC Web of Conferences, 2017, 90. 01064.
3. F. E. Gunawan, H. Homma, S.S. Brodjonegoro, A.B. Hudin and A. Zainuddin, Mechanical Properties of Oil Palm Empty Fruit Bunch Fiber, Journal of Solid Mechanics and Materials Engineering, 3(7), 2009, pp. 943-951.
4. M.Z. Mohamed Yusoff, S.M Sapuan, and N. Ismail, Tensile Properties of Single Oil Palm Empty Fruit Bunch (OPEFB) Fibre, Sains Malaysiana. 38(4), 2009, pp. 525–529.
5. C.S. Hassan, C.W. Yeo, B.B. Sahari, S.M. Sapuan, and N. Abdul Aziz, Mechanical Properties of Unidirectional Oil Palm Empty Fruit Bunch (OPEFB) Fiber Reinforced Epoxy Composite, IOP Conference Series: Materials Science and Engineering, 206, 2017, 012045.
6. B, Sajimsha, Analysis of Mountain Bike Frames by ANSYS. International Journal for Research in Applied Science and Engineering Technology, 7, 2019, pp. 1167-1175.
7. J.M. Whitney and M.B. Riley, (1996). Elastic Properties of Fibre Reinforced Composite Materials, AIAA Journal, 4(9), 1966, pp. 1537–1542.
8. A.P.S. Selvadurai and H. Nikopour, Transverse Elasticity of a Unidirectionally Reinforced Composite with an Irregular Fibre Arrangement: Experiments, Theory and Computations, Composite Structures. 94(6), 2012, pp. 1973–1981.
9. M.D. Isaac and I. Ori, Engineering Mechanics of Composite Materials, 2nd Edition, Oxford University Press, 2006.
10. T.J-C. Liu and H-C. Wu, Fiber Direction and Stacking Sequence Design for Bicycle Frame Made of Carbon/Epoxy Composite Laminate, Materials & Design, 31(4), 2010, pp. 1971-1980.
11. Y. Hu, Y. Xiao, W. Shang, and J. Zhang, Effect of Fibre Direction and Stacking Sequence on Dynamic Impact Performance of Composite Bicycle Frame, International Journal of Crashworthiness, 22(5), 2017, pp. 556-564.
12. H. Jung, J.A. Lee, K.Y. Kim, and H. Chun, Determination of Number of Layers and Stacking Sequence of Composite Bicycle Frame., Advanced Materials Research, 123-125, 2010, pp. 531-534.
13. H.J. Chun, J.A. Lee, and K.T. Kang, Study of Design Variable with Loading Condition for Composite Laminate Bicycle Frame. In ECCM 2012 - Composites at Venice, Proceedings of the 15th European Conference on Composite Materials (ECCM 2012 - Composites at Venice, Proceedings of the 15th European Conference on Composite Materials), European Conference on Composite Materials, ECCM, 2012.
14. P. Sarath, A. Deepak, H, Hrishikesh, N.S. Daniel and Jinuchandran, Stress Analysis of Bicycle Frame using Different Materials by FEA, GRD Journals for Engineering, 6(7), 2021, pp. 14-20.

Authors Introduction

Mr. Too Kok Sem

He received his Bachelor's degree in Mechanical Engineering in 2022 from the Faculty of Engineering, Technology & Built Environment, UCSI University, Malaysia.

Dr. Cik Suhana Hassan

She received her bachelor's and master's degrees in 2009 and 2011, respectively, from Universiti Teknologi PETRONAS, and her PhD in 2019 from Universiti Putra Malaysia. She is currently an Assistant Professor at the Department of Mechanical and Mechatronics Engineering of UCSI University. Her research interests include the investigation of bio-composites characteristics for applications, particularly automotive.

Ms. Nor Fazilah Abdullah

She received her Bachelor's degree in aerospace engineering (Hons) from IIUM, Gombak in 2010 and her Master's degree in Mechanical Engineering from UKM, Bangi in 2015. Currently she is pursuing Doctoral of Philosophy programme at UCSI University, Kuala Lumpur. Her research interest in bio-based nanoparticles materials.

Ammar Abdulaziz Al Talib

Dr. Ammar Al Talib has finished his B.Sc and M.Sc degrees in Mechanical Engineering from the University of Mosul/Iraq.
He has finished his Ph.D degree from UPM University / Malaysia.
He is also is a Chartered Engineer and Member of the Institute of Mechanical Engineers / UK. (CEng. MIMechE). He has developed all the Postgraduate Programs at the Faculty of Engineering at UCSI University / Malaysia and worked as the Head of Postgraduate and Research department at the same faculty for the years 2010-2018.